Victoria-Hernandez, J.; Hernandez-Silva, D.; Yi, S.; Letzig, D.; Bohlen, J.:
Intermediate temperature deformation behaviour of fine grained AZ61 alloy processed by hydrostatic extrusion
In: Materials Science and Engineering A (2011) Elsevier

DOI: 10.1016/j.msea.2011.09.104

Intermediate temperature deformation behaviour of fine grained Mg-Al-Zn alloys processed by hydrostatic extrusion

J. Victoria-Hernandez[1*], D. Hernandez-Silva[1], S. B. Yi[2], D. Letzig[2], and J. Bohlen[2]

[1] *Department of Metallurgical Engineering, Instituto Politécnico Nacional-ESIQIE, Apdo. Postal 118-392, 07738 Mexico City, Mexico*
[2] *Magnesium Innovation Centre MagIC, Helmholtz-Zentrum Geesthacht, Max-Planck-Strasse 1, D.21502 Geesthacht, Germany.*

Abstract:

In this work, the intermediate temperature deformation behaviour of AZ31 and AZ61 alloys processed by hydrostatic extrusion has been examined. By means of this thermomechanical process it is possible to refine the microstructures of the AZ31 and AZ61 alloys to generate average grain sizes of 2.3 and 3.5 µm respectively. The evolution of microstructure and texture after tensile testing at 175, 200 and 225 °C in air at three different strain rates of 10^{-2}, 10^{-3} and 10^{-4} s^{-1} was investigated. It was found that both alloys exhibit low temperature superplasticity, at 200 °C for AZ31 and at 175 °C for the AZ61 alloy. The maximum elongation recorded for AZ31 was 395 % at 225 °C and 10^{-4} s^{-1}, and 540 % for AZ61 tested at 225 °C and $1.5 \cdot 10^{-3}$ s^{-1}. The intermediate temperature deformation behaviour is explained by the combination of three different mechanisms: I) dislocation creep, II) low temperature dynamic recrystallisation (LTDRX) and III) grain boundary sliding (GBS).

Keywords: Superplasticity, texture, deformation mechanisms, LTDRX, GBS.

1. INTRODUCTION

The low density of magnesium makes it attractive for lightweight components used principally in the automotive and aeronautic industries. Over the last 20 years, great advances in magnesium research have been made [1]. Although wrought alloys generally exhibit better mechanical properties than cast alloys, most commercial applications still utilise components produced by casting. Wrought magnesium alloys have so far found limited application, mainly as a result of their poor formability at low temperatures close to room temperature. This low formability is due to the hexagonal crystal structure and the limited number of deformation modes available near room temperature [2]. Much work has been carried out in order to improve the formability and mechanical properties of wrought magnesium alloys. Current research in this area is concerned with the development of new alloy systems, the understanding of the deformation mechanisms involved during the deformation of polycrystalline magnesium alloys and on thermomechanical treatments that allow the microstructure and formability at low temperatures to be improved [3-8].

* Corresponding author. Tel.: +52 55 57296000x54214
E-mail address: jvhciber@hotmail.com (J. Victoria-Hernandez)

Superplasticity refers to the ability of a material to reach very large elongations, as a rule-of-thumb a strain of at least 200%, when a sample is pulled in tension [9]. Superplastic Forming (SF) provides the capability to form complex parts that are difficult to form in the non-superplastic region. By definition, superplasticity enables certain metals and alloys to achieve extended ductility but under specific, restricted circumstances: 1) low strain rates usually between 10^{-5} to 10^{-3} s^{-1}, 2) fine and stable microstructures and 3) a deformation temperature around 0.5 T_m or higher (where T_m is the absolute melting temperature) [10]. Under these conditions, the steady state during uniaxial tensile deformation of superplastic materials can be described by the power law:

$$\sigma = K \cdot \dot{\varepsilon}^m \qquad (1)$$

where σ is the flow stress, $\dot{\varepsilon}$ is the strain rate, K is a constant and *m* is the strain rate sensitivity that should be higher than 0.3 [11].

Superplastic behaviour in Mg alloys has been observed by various authors, see Table 1. The results summarised in the upper part of Table 1 refer to investigations in which conventional thermomechanical treatments (rolling and extrusion) were used. It is interesting to note that the temperatures used during superplastic deformation were higher than $0.5T_m$ and that the average grain sizes were between 6 and 25 μm. The *m* values reported in these investigations were about 0.5. It is known that a high value of *m* retards flow localisation, and therefore, the ductility is generally high [12]. With $m > 0.3$, Grain Boundary Sliding (GBS) is the mechanism that controls deformation and this is related to the superplastic behaviour of materials. Conversely, if *m* values are lower than 0.3 the ductility is usually low and dislocation creep processes are activated [12, 17]. However, by means of Severe Plastic Deformation techniques (SPD), fine or ultra-fine microstructures (grain sizes < 1 μm) can be attained. This reduction in grain size enables *m* values > 0.3 to be obtained at temperatures lower than 0.5 T_m. This corresponds to a phenomenon called low temperature superplasticity (LTSP). The results of some of these studies are summarised in the lower part of Table 1.

Recently, Swiostek et al. [22] showed that hydrostatic extrusion (HE) is a feasible thermomechanical treatment for the production of fine-grained magnesium alloys. During HE, a hydrostatic medium presses on to the billet. The pressure is developed from a ram and passed on to the medium leading to hydrostatic pressure on all sides of the billet to make it flow through the die. This extrusion process enables finer grains and higher extrusion rates at lower extrusion temperatures than the conventional direct or indirect extrusion processes [23]. The application of such a low temperature process and the potential for low temperature superplasticity are especially attractive features in magnesium alloys because of their poor formability near room temperature.

In this paper, hydrostatically extruded round bars of AZ31 and AZ61 are used to reveal the operative deformation mechanisms during low temperature superplastic deformation and the evolution of microstructure and texture.

Table 1: Superplasticity in Mg-based alloys processed by different methods.

2. EXPERIMENTAL PROCEDURE

Two magnesium alloys were selected: AZ31 and AZ61. Direct chill-cast billets with 0.8 m diameter were homogenized for 12 hr at 350 °C and then cooled down in air to room temperature. Hydrostatic extrusion of both alloys was carried out at 150 °C using an extrusion ratio of 1:28 and an extrusion rate of 0.13 ms^{-1} to produce bars of 0.015 m in diameter. The extruded bars were water quenched after the extrusion process. Details of the hydrostatic extrusion process can be found elsewhere [22-24].

The thermal stability of the microstructure and texture were evaluated by static annealing experiments. Samples from the extruded bars of 0.015 m in diameter and 0.02 m in height were heated to temperatures of 175, 200 and 225 °C for 5 and 60 minutes respectively.

Quantitative texture measurements on both as-extruded and heat treated samples were carried out with a Panalytical™ x-ray diffractometer in reflection geometry using Cu-Kα radiation. Six pole figures, (00.2), (10.0), (10.1), (10.2), (10.3) and (11.0) were measured up to a tilt angle of 70 °. The data were used to calculate the complete orientation distribution function. Recalculated inverse pole figures in the extrusion direction are used to characterise the texture of the bars. Due to the symmetry of the round bar extrusion, the inverse pole figures (IPF) in the extrusion direction contain all the necessary information to describe the texture [24].

Tensile samples with a gauge length of 20 mm and a diameter of 6 mm, oriented with their longitudinal axis parallel to the extrusion direction, were machined from the extruded bars. Tensile tests were conducted at 175, 200 and 225 °C in air using a universal testing machine (Zwick™ Z050) equipped with an electrical furnace. At each temperature, three different strain rates were used 10^{-2}, 10^{-3} and 10^{-4} s^{-1}. An extensometer was attached to the samples to assure an accurate measurement of strain. This extensometer also controlled the strain rate during the whole test. Before starting the test, the samples were held at the selected temperature for 10 min in order to ensure a homogeneous and stable temperature. When failure occurred,

the specimens were immediately quenched into water, in order to retain the microstructure and texture at the moment of fracture.

Specimens for optical microscopy were sectioned, cold mounted, polished with oxide polishing suspension (OPS) of 0.5µm and finally etched in an acetic-picral solution [25]. Grain sizes were measured with the linear intercept method.

The microstructure and texture after deformation were characterized using Electron Backscatter Diffraction (EBSD) in a field emission gun scanning electron microscope (Zeiss ™, Ultra 55) equipped with an EDAX/TSL EBSD system with a Hikari detector. The samples were prepared from the fractured specimens. These were mechanically polished with 1 µm alumina powder and then electro-chemically polished using a Struers™ AC2 solution at 16 V for 80 s. EBSD measurements were made near the fracture tip using an accelerating voltage of 15 kV and a step size of 0.2 µm.

3. RESULTS AND DISCUSSION

3.1 Microstructural analysis

Fig. 1 shows the microstructures and inverse pole figures of the as-extruded AZ31 and AZ61 alloys. The microstructure of the AZ31 alloy (Fig. 1a) is rather inhomogeneous and is composed of large, elongated, unrecrystallised grains surrounded by new, fine and recrystallized grains. The average grain size is about 2.3 µm. Due to the low extrusion temperature and the fact that the extruded bars were quenched in water, static recrystallisation and grain growth were stopped immediately after processing. Fig 1b exhibits the corresponding IPF of AZ31 after extrusion. In general, a strong texture with a (10.0) fibre component is found. Such a texture results in the distinct alignment of the (00.1) basal planes parallel to the extrusion direction as is often found in symmetrical extrusions of magnesium alloys. This phenomenon was observed by Bohlen et al. [24] in AZ31 processed by HE at 225, 250 and 300 °C. The results were explained by the incomplete recrystallisation process and the results for HE at 150 °C observed in the present investigation compare well with these findings.

The microstructure of the AZ61 alloy appears to be more homogeneous and well recrystallised (Fig. 1c). The average grain size is 3.5 µm and the dark bands observed in the micrograph correspond to regions where a high concentration of the secondary phase $Mg_{17}Al_{12}$ can be found. Fig. 1d, shows the corresponding IPF of AZ61 which differs from that of AZ31. The intensity of the ⟨10.0⟩ pole is weaker than in the AZ31 alloy and a further ⟨11.0⟩ pole is visible. This reduction of the intensities can be attributed to the more complete recrystallisation process in AZ61 compared to AZ31. Mackenzie et al. [26] reported that unrecrystallised grains are mainly oriented towards the ⟨10.0⟩ pole, whereas most of the recrystallised grains tend to orient preferentially towards the ⟨11.0⟩ pole. This can explain the double fibre and weaker texture intensity found in the AZ61 alloy.

Fig. 1. Microstructure and inverse pole figures of the as-extruded alloys. a) and b) AZ31 and, c) and d) AZ61.

The average grain sizes of the AZ31 and AZ61 alloys after annealing for 5 and 60 min at different temperatures are depicted in Fig. 2. Both alloys show good microstructural stability and no significant changes in grain size were observed.

Fig. 2. Average grain sizes of the extruded AZ31 and AZ61 alloys as a function of the annealing temperature.

3.2 Mechanical testing

The true stress-true strain curves for AZ31 and AZ61 tested at temperatures of 175, 200 and 225 °C and a strain rate of 10^{-3} s^{-1} are presented in Fig. 3. In general, the flow stress decreases with increasing temperature in both alloys. After reaching a peak stress, both alloys exhibit flow softening which is typically related to dynamic recrystallisation (DRX) [27] as found previously in Mg alloys. For example, Al-Samman et al. [28] performed compression tests at 200, 300 and 400 °C and showed that DRX plays an important role in the deformation of the AZ31 alloy, especially at 200 °C, because at temperatures lower than 225 °C high critical stresses are necessary for the activation of non-basal slip systems. Yi et al. [29] performed tensile tests on extruded AZ31 alloys with average grain sizes of 4 μm at temperatures between 150 and 250 °C. The results showed changes in mechanical behaviour and elongations to failure of about 150 % when the temperature was increased to 250 °C. These results were explained by the high activity of ⟨c+a⟩ slip systems and the occurrence of extensive rotational DRX during the test. In both studies, the flow softening observed during compression or tension was explained by the effect of DRX. However in the current work, flow softening was observed even at 175 °C in both alloys. The reduction in flow stress is observed for all strain rates used. This reduction is less pronounced in AZ31 (see Fig. 3a), whereas in AZ61 the reduction in flow stress is continuous until the end of the tests where low stresses were recorded without abrupt failure (see Fig. 3b).

Fig. 3. Stress-strain curves at 175, 200 and 225 °C and 10^{-3} s^{-1}. a) AZ31 and b) AZ61

The decrease of the flow stresses changes during the tests. Starting at the maximum stress the slope of the curves increases up to a maximum slope before it changes again. This change in the slope of the curves during the flow softening was observed in the range of ~0.4 or 0.6 true strain in both alloys. It is clearly visible for AZ61 in Fig. 3b whereas it is only obvious for AZ31 tested at 225°C in Fig. 3a. Something similar was reported by Tan et al. [30]. In that work, it was pointed out that DRX takes place during the first 60% of engineering strain (~ 0.4 of true strain) when a sample was tested in tension at 250 °C. By means of DRX, the microstructure was refined from 12 µm in the as rolled condition, to 6 µm, after 60% strain. At higher strains the slope of the curves increases again when strain localisation starts.

Fig. 4. Elongation to failure vs. strain rate for AZ31 and AZ61 alloys tested at 175, 200 and 225 °C (full and empty symbols for AZ31 and AZ61 respectively).

The results of elongation to failure vs strain rate for the AZ31 and AZ61 alloys in the current study are depicted in Fig. 4. It can be seen that the maximum elongation of about 400 % for AZ31 was achieved at 225 °C and 10^{-4} s^{-1}. This result fits well with the behaviour reported by Lee et al. [31] for extruded sheets of an AZ31 alloy tested at the low strain rate of 10^{-4} s^{-1} and temperatures around 225 °C. In general for the AZ31 alloy, when the strain rate was increased further, the total elongation decreased monotonically at all temperatures. In the case of AZ61, an elongation to failure of about 160 % was recorded at the high strain rate of 10^{-2} s^{-1}. Interestingly, the maximum elongation was observed at 200 °C and 10^{-3} s^{-1} instead of 225 °C with the same strain rate. It would be expected that the higher temperature would give better conditions for the superplastic phenomenon [11]. In order to determine the strain rate at which the maximum elongation is obtained, two more strain rates, $1.5x10^{-3}$ and $2x10^{-3}$ s^{-1}, were used at 225 °C. It was found that the maximum elongation to failure of 540 % for AZ61 tested at 225°C was achieved at a strain rate of $1.5x10^{-3}$ s^{-1}. On the other hand, if the strain rate is decreased to 10^{-4} s^{-1}, the alloy showed lower elongations at 200 and 225 °C. Conversely, at 175 °C the elongation to failure increased monotonically as the strain rate was reduced. At this temperature and a strain rate of 10^{-4} s^{-1} the alloy showed excellent superplastic behaviour, reaching a total elongation to failure of about 520 %.

The logarithm of flow stress vs. logarithm of strain rate is plotted in Fig. 5. The flow stress for each condition was taken from the stress peak. The flow stresses of the alloys increase as the temperature is reduced and the strain rate is increased. The strain rate sensitivity (m) values were estimated from the slope of the graph. Both alloys exhibited low m values in the range 0.10 to 0.30 for AZ31 and 0.11 to 0.25 for AZ61. These low m values can be related to dislocation creep processes especially for AZ61 [12]. The

power law condition with m=0.3 was only accomplished by AZ31 in the strain rate range 10^{-3} to 10^{-4} s^{-1} at 200 and 225 °C.

With stress exponents (n=1/m) ranging from 6-9 for the AZ61 alloy, the simple power-law breakdown and superplasticity should not be observed [5, 31, 32].

Fig. 5. Flow stress vs. strain rate for the AZ31 and AZ61 alloys tested at 175, 200 and 225 °C (Full and empty symbols for AZ31 and AZ61 respectively).

For this reason, further analysis of the flow stresses was carried out. Based on the fact that a significant reduction in the flow stresses was observed at around 0.5 true strain for all testing conditions used in this study, the m values were calculated at this strain. The results revealed that m increases at all temperatures for AZ61. The m values calculated at 0.5 true strain are plotted in Fig. 6.

Fig. 6. Flow stress at 0.5 strain vs. strain rate for AZ61 tested at 175, 200 and 225 °C.

3.3 Microstructure and texture

In order to reveal the microstructural characteristics of the deformed samples of AZ61, tests up to 0.2 and 0.5 true strain were performed at 200 ^{o}C and 10^{-4} s^{-1}. Although, the recrystallisation process started before a true strain of 0.2, a duplex microstructure is found, where grains resulting from the extrusion process are now surrounded by new and fine recrystallised grains (Fig. 7a). However, after reaching a true strain of 0.5 a fully recrystallised and homogeneous microstructure is observed (7b). This fact could give the necessary conditions to activate GBS and continue the deformation process in superplastic-like behaviour.

Fig. 7. Optical micrographs of samples of the AZ61 alloy deformed in tension at 200 ^{o}C and 10 $^{-4}$ s^{-1}: a) 0.2 true strain and b) 0.5 true strain.

Micrographs depicting the morphological characteristics of the gauge surfaces of the samples of both alloys showing the maximum elongation are presented in Fig. 8. In both samples the grains seem to rotate during the deformation process. This morphology is often observed when grain boundary sliding is the rate-controlling mechanism [8, 17, 30]. Bieler et al. [33] demonstrated that this kind of morphology corresponds to grain boundary sliding as the main mechanism during superplastic deformation of mechanically alloyed aluminium in which the strain rate sensitivity was 0.5. However, it is interesting to note that the *m* values measured in this investigation for samples of both alloys that showed superplastic-like behaviour are 0.3

Fig. 8. Surface appearance of superplastically deformed samples. a) AZ31 at 225 °C and 10^{-4} s^{-1} and b) AZ61 at 225 °C and 10^{-3} s^{-1}

Orientation maps for samples tested at 175 and 225 °C and 10^{-3} s^{-1} are presented in Fig. 9a and b for the AZ31 alloy, and c and d for the AZ61 alloy. These conditions were selected because at 175°C both alloys are located in the non-superplastic region and at 225 °C both alloys showed superplastic behaviour.

At 175 °C, significant grain refinement occurred in both alloys due to DRX (see Fig, 9a and 9c). Taking into account the melting temperature of pure Mg of ~ 650 °C, the recrystallisation observed in this investigation can be referred to as low temperature dynamic recrystallisation (LTDRX). It is noteworthy that the final microstructure is homogeneous, in the case of the AZ31 alloy. All the elongated grains observed after the extrusion process became fully recrystallised during the tensile test and the final average grain size was about 1.5 µm. Under superplastic conditions, i.e. testing at 225 °C and 10^{-3} s^{-1}, different microstructures were found in AZ31 and AZ61 (see Fig. 9b and d). Although AZ61 experienced an elongation to failure about twice that of AZ31, the final microstructure seems to be more equiaxed compared to AZ31. At 225 °C cavity formation and extensive precipitation took place especially in the AZ61 alloy (note the black areas in Fig. 9d).

Fig. 9. Orientation maps for samples tested at 175 and 225°C at a constant strain rate of 10^{-3} s^{-1}. a) and b) AZ31, c) and d) AZ61.

The final average grain sizes of AZ31 and AZ61 for all conditions tested are presented in Fig. 10. It can be seen for AZ31 (Fig. 10a) that when the temperature is increased or the strain rate is decreased the average grain size increases monotonically. In the case of the alloy AZ61 tested at 175 and 200 °C at a strain rate of 10^{-2} s^{-1} (Fig. 10b) only a partially recrystallised microstructure is observed. It is interesting to note that in the AZ31 alloy tested under the same conditions fully recrystallised microstructures were produced. If only the recrystallised grains are considered (by limiting the grain size measurements to grains which have an internal orientation spread less than 1° [34]), the influence of temperature and strain rate is the same as for AZ31. Especially for the low strain rate of 10^{-4} s^{-1}, the average grain size is comparable in the two alloys and therefore does not explain the distinct differences in the elongation to failure observed.

Fig. 10. Average grain sizes after deformation at different temperatures as a function of the strain rate: a) AZ31 and b) AZ61. (Full symbols refer to all grains whereas open symbols refer to recrystallised grains only)

It is well known that to maintain a fine grain size in the superplastic forming range, the presence of a second phase or particles at the grain boundaries is required [35]. An inspection of the distribution of precipitates in samples of AZ61 deformed under the low strain rate condition revealed that fine and well distributed precipitates remain during testing at 175 °C (Fig 11a). However, as the temperature is increased to 225 °C the nucleation of coarse precipitates takes place (Fig. 11b). The growth of these particles under these conditions corresponds to the appearance of cavities as seen in Fig. 9. These effects can explain why the elongation to failure was reduced in this range.

Fig. 11. SEM micrographs of precipitate distributions in AZ61 deformed superplastically at 10^{-4} s^{-1}. a) 175 °C and b) 225 °C

The IPF's for samples tested at 175 and 225 °C and 10^{-3} s^{-1} are presented in Fig. 12 for both alloys. The IPF for AZ31 (Fig. 12a) shows randomization of the texture in which the $\langle 2\bar{1}\bar{1}0 \rangle$ component became visible compared to the as-extruded condition where the $\langle 10\bar{1}0 \rangle$ fibre component dominates the texture. As the temperature was increased and the material underwent superplastic deformation, the material developed a weak texture and the intensity of the $\langle 2\bar{1}\bar{1}0 \rangle$ pole increases (Fig. 12b).

Fig. 12. IPFs of samples tested at 175 and 225°C and a constant strain rate of 10^{-3} s^{-1}. a) and b) AZ31 and c) and d) AZ61.

Fig. 12c exhibits the IPF of AZ61 after testing in the non-superplastic regime. A weak texture with the double fibre components remains after 180 % elongation. It is worthwhile to note that a very similar distribution was observed in the as-extruded condition, whereas, in the superplastic region an almost random distribution was found (see Fig. 12d). This reduction in intensities is often related to GBS taking place during superplastic deformation causing randomization of the texture [31]. It is noteworthy that in this extremely weak texture the highest intensities are not found along the arc between the $\langle 2\bar{1}\,\bar{1}0 \rangle$ pole and $\langle 10\bar{1}0 \rangle$ poles but are found between the $\langle 10\bar{1}0 \rangle$ and the $\langle 2\bar{1}\,\bar{1}1 \rangle$ poles. Such textures are sometimes found in extruded Mg alloys containing rare earth elements, as for example described by Bohlen et al. [34], Stanford et al. [36, 37] and Cottam et al. [38] This explicit aspect of this work will be treated in a separate paper Victoria-Hernandez et al. [39].

4. CONCLUSIONS

It is possible to observe superplastic behaviour at low temperatures in fine-grained Mg-Al-Zn alloys processed by hydrostatic extrusion at 150 °C. The lowest temperature at which superplasticity was observed was 0.35 T_m for AZ31 and 0.33 T_m for AZ61.

As a result of low temperature dynamic recrystallisation, significant flow softening was observed during the tests. LTDRX enables the transition from dislocation creep processes to grain boundary sliding that results in enhanced plasticity of the AZ31 and AZ61 alloys. Although the strain rate sensitivities recorded in the superplastically deformed samples were lower than 0.3, the combination of the flow softening due to DRX and the effect of grain boundary sliding allows superplastic behaviour at low temperatures in Mg-Al-Zn alloys to be observed.

Extensive conglomeration of precipitates and the concurrent appearance of cavities reduced the superplastic performance of AZ61 at low strain rates.

During tensile deformation, texture randomization was observed in both alloys. Slightly weaker intensities were recorded for AZ61 than for AZ31. This can be related to the larger elongations to failure achieved in AZ61. The underlying mechanisms that are active to reveal this condition include grain boundary sliding. Furthermore, texture development includes the formation of grain orientations that so far have mainly been observed in rare earth containing Mg alloys.

Acknowledgments

The authors would like to thank Dr. P.A. Beaven at the Helmholtz-Zentrum Geesthacht for his comments and intensive discussion.

JVH is grateful with CONACyT Mexico for the economic support for the stay in Germany and with the technician staff of the WZW group at Helmholtz Zentrum Geesthacht in Germany for samples preparation.

References

[1] S.B. Yi, H.G. Brokmeier, R. E. Bolmaro, K.U. Kainer and T. Lippmann, Scripta Mater. 51 (2004) 455-460
[2] K. Hantzsche, J. Bohlen, J. Wendt, K.U. Kainer, S.B. Yi and D. Letzig, Scripta Mater. (2010), doi:10.1016/j.scriptamat.2009.12.033
[3] J. Bohlen, P. Dobron, E. Meza-Garcia, F. Chmelik, P. Lukac, D. Letzig and K.U. Kainer. Adv. Eng. Mat., doi:10.1002/adem.200600023
[4] W.J. Kim, M.J. Kim and J.Y. Wang, Mater. Sci. Eng. A 516 (2009) 17-22
[5] H.J. Frost, M. F. Ashby, Deformation Mechanism Maps, Pergamon Press, Oxford, 1982
[6] S. Spigarelli, Mater. Sci. Eng. A 492 (2008) 153-160
[7] S. Q. Zhu, H.G. Yan, W. J. Xia, J.Z. Liu and J.F. Jiang, J. Mater. Sci. 44 (2009):3800-3806
[8] S.W. Lee, Y.L. Chen, H.Y. Wang, C.F. Yang and J.W. Yeh, Mater. Sci. Eng. A 464 (2007) 76-84
[9] H. Watanabe, M. Fukusumi, H. Somekawa and T. Mukai, Mater. Sci. Eng. A(2010), doi: 10.1016/j.msea.201006.053
[10] K. S. Raghavan, Superplasticity, Bull. Mater. Sci., Vol. 6, No. 4, 1984
[11] K.A. Padmannabhan, R.A. Vasin and F.U. Enikeev, Superplastic Flow Phenomenology and Mechanics, Springer-Verlag Berlin Heidelberg 2001
[12] P. Panicker, A.H. Chokshi, R. K. Mishra, R. Verma and P.E. Krajewski, Acta Mater. 57 (2009) 3683-3693
[13] W.J. Kim, J.D. Park, U.S. Yoon, J. Alloys and Compounds, 464 (2008) 197-204
[14] H. Watanabe, M. Fukusumi, Mater. Sci. Eng. A 477 (2008) 153-161
[15] W.J. Kim and S.W. Chung, Metals and Materials, Vol. 6, No. 3 (2000)
[16] H. Watanabe, T. Mukai, M. Kohzu, S. Tanabe and K. Higashi, Acta Mater. 47,(1999) 3753-3758
[17] H. Watanabe, T Mukai, K. Ishikawa, M. Mabuchi and K. Higashi, Mater. Sci. Eng. A 307(2001) 119-128
[18] Y. Miyahara, Z. Horita and T.G. Langdon, Mater. Sci. Eng. A 420 (2006) 240-244
[19] M. Mabuchi, K. Ameyama, H. Iwasaky and K. Higashi, Acta Mater. 47 (1999) 2047-2057
[20] W.J. Kim, M.J. Kim and J.Y. Wang, Mater. Sci. Eng. A 527 (2009) 322-327
[21] A. Galiev, R. Kaibyshev, Scripta Mater. 51 (2004) 89-93
[22] J. Swiostek, J. Goken, D. Letzig and K.U. Kainer, Mater. Sci. Eng. A 424 (2006) 223-229
[23] J. Goken, J. Swiostek, D. Letzig and K.U. Kainer, Mater. Sci. Forum. 482 (2005) 387-390
[24] J. Bohlen, S.B. Yi, J. Swiostek, D. Letzig, H.G. Brokmeier and K.U. Kainer, Scripta Mater. 53 (2005) 259-264
[25] V. Kree, J. Bohlen, D. Letzig and K.U. Kainer, Pract. Metall. 41 (2004) 233
[26] L.W.F. V. Mackenzie, G.W. Lorimer, F.J. Humphreys, T. Wilks, Mater. Sci. Forum 477-82 (2004) .
[27] C.M. Sellars, Mat. Sci. and Tech. 6 (1990) 1072-1081
[28] T. Al-Samman, G. Gottstein, Mater. Sci. Eng. A 490 (2008) 411-420
[29] S.B. Yi, S. Zaefferer, H. G. Brokmeier, Mater. Sci. Eng. A 424 (2006) 275-281
[30] J.C. Tan, M.J. Tan, Mater. Sci. Eng. A339 (2003) 81-89
[31] W.J. Kim, S. W. Chung, C.S. Chung and D. Kum, Acta Mater. 49 (2001) 3337-3345
[32] H.W. Hayden, S. Floreen, P.D. Goodell, Metall. Trans. 3 (1972) 833
[33] T.R. Bieler, T.G. Nieh, J, Wadsworth and A.K. Muhkerjee, Scripta Metall. 22 (1988) 851-855
[34] J. Bohlen, S.B. Yi, D. Letzig, K.U. Kainer, Mater. Sci. Eng. A (2010), doi:10.1016/j.msea.2010.07.081
[35] T.G. Nieh, J. Wadsworth and O.D. Sherby, Superplasticity in metals and ceramics, Cambridge University Press, 1997, p. 23
[36] N. Stanford, M. Barnett, Scripta Mater. 58 (2008) 179-182
[37] N. Stanford, M. Barnett, Mater. Sci. Eng. A 496 (2008) 399-408
[38] R. Cottam, J. Robson, G. Lorimer, B. Davis, Mater. Sci. Eng. A 485 (2008) 375-382
[39] J. Victoria-Hernandez, S.B. Yi, D. Letzig and J. Bohlen, in preparation.

Alloy	Grain size (μm)	T (^{o}C)	T/Tm	$\dot{\varepsilon}$ (s^{-1})	ε to failure (%)	*m*	Processing method	Reference
Conventional superplasticity (>0.5Tm)								
AZ31	8.1	400	0.70	10^{-4}	475	~0.5	Rolling	[12]
AZ31	6.6	400	0.70	$2x10^{-4}$	800	0.56	Strip Casting+Rolling	[13]
AZ31	Mixed 8-25	450	0.79	10^{-5}	596	0.5	Extrusion	[14]
AZ61	8.7	400	0.76	$2x10^{-4}$	400	0.5	Hot Rolling	[15]
AZ61	~20	375	0.71	10^{-5}	~450	0.5	Rolling	[16]
Low temperature superplasticity (≤0.5Tm)								
AZ31	0.7	150	0.26	10^{-4}	460	-	Extrusion+ECAP	[14]
AZ61	0.3-0.5	250	0.47	$3x10^{-4}$	850	0.37	Differential Speed Rolling (DSR-SPD)	[23]
AZ61	~0.6	200	0.38	$3.3x10^{-4}$	1320	0.3	Extrusion +ECAP	[18]
AZ91	0.5	200	0.42	$5x10^{-5}$	~600	0.5	ECAE	[19]
ZK60	1.4	250	0.48	10^{-3}	~1000	0.5	High Ratio DSR-SPD	[20]
ZK61	3.7	250	0.48	$1.4x10^{-4}$	1330	~0.45	Isothermal Rolling	[21]
ZK61	~0.7	200	0.38	10^{-3}	659	0.5	Powder Metallurgy (PM)	[17]

Table 1: Superplasticity in Mg-based alloys processed by different methods.

Figure(s)

Click here to download high resolution image

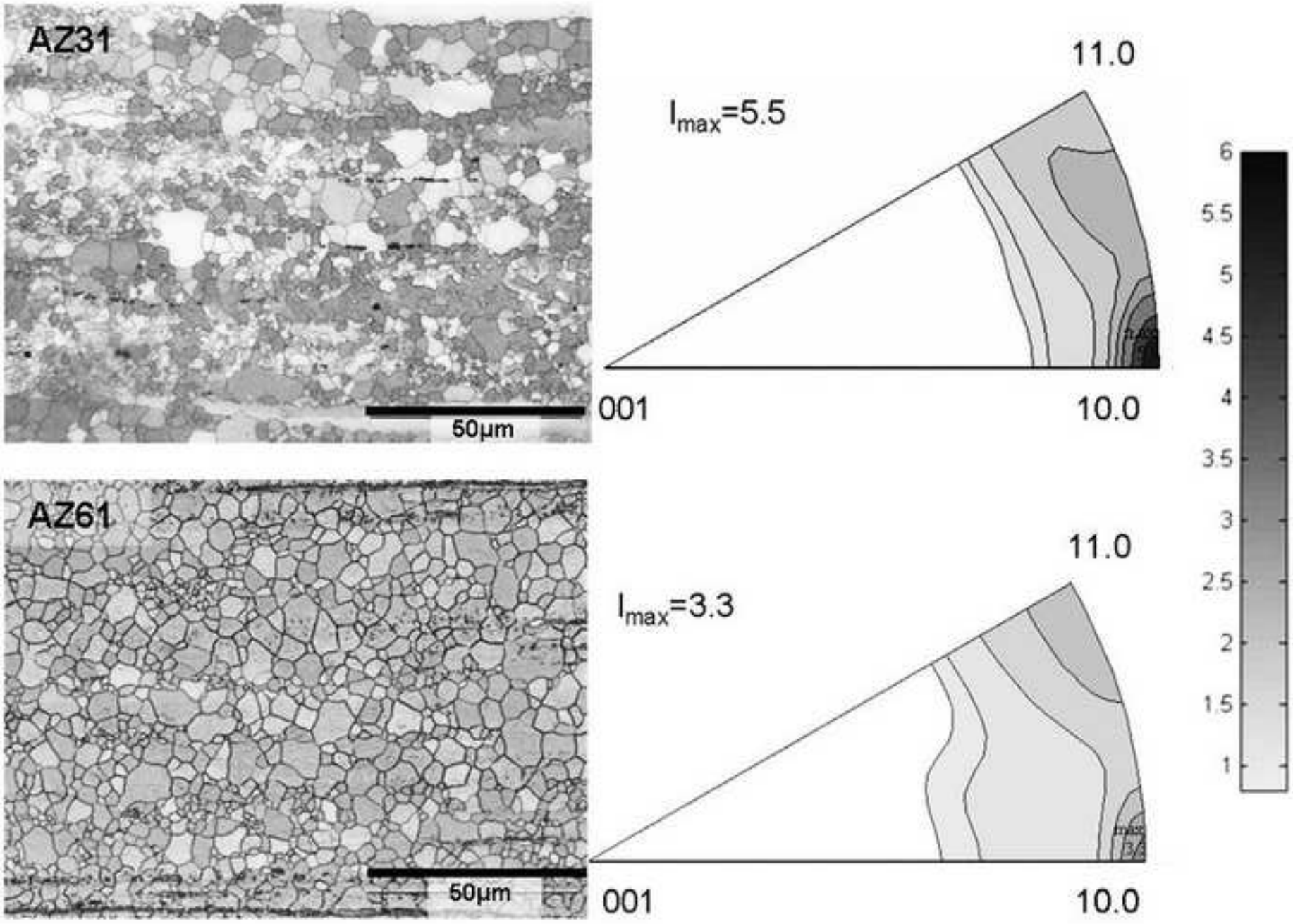

Figure(s)

Click here to download high resolution image

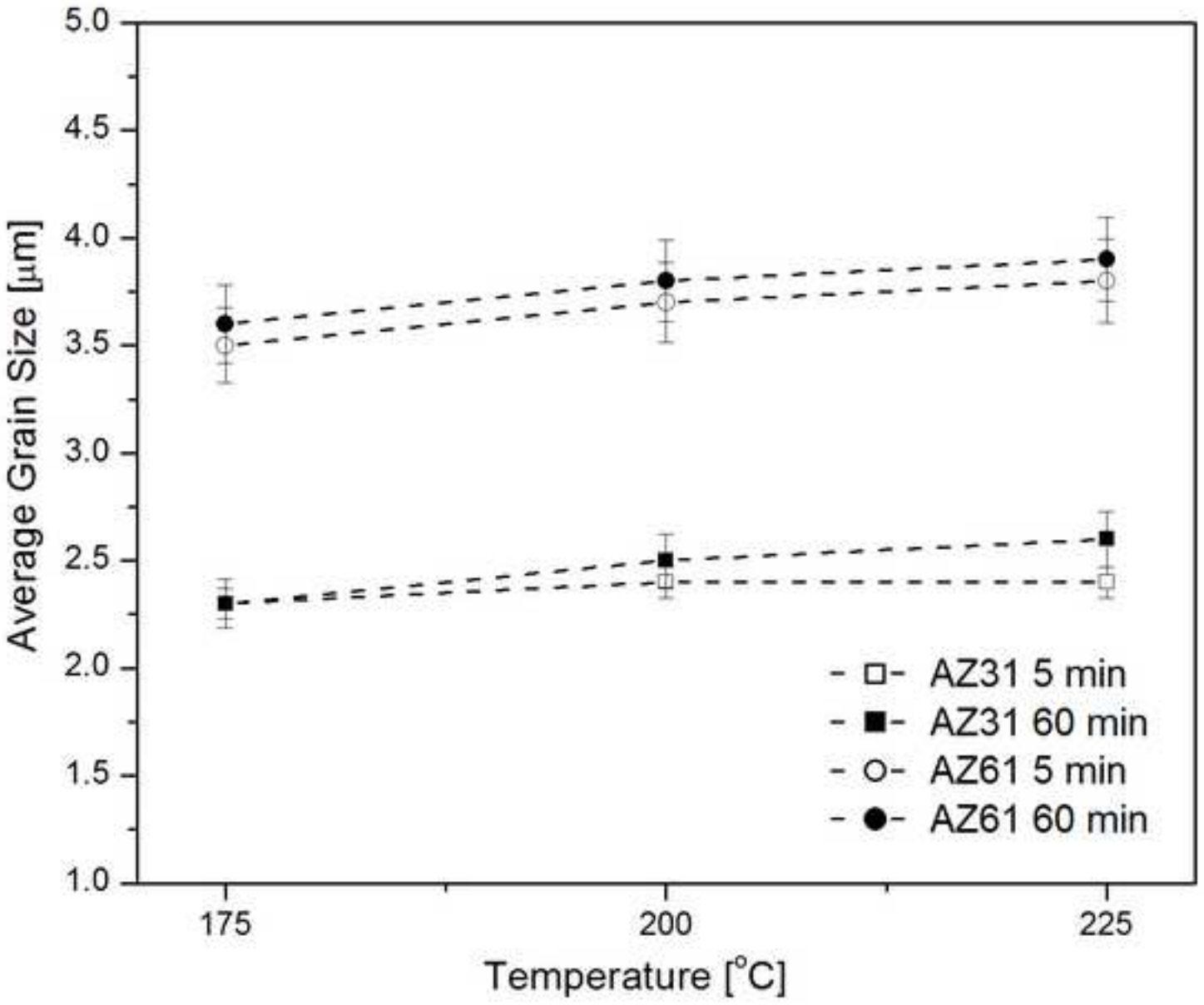

Figure(s)

Click here to download high resolution image

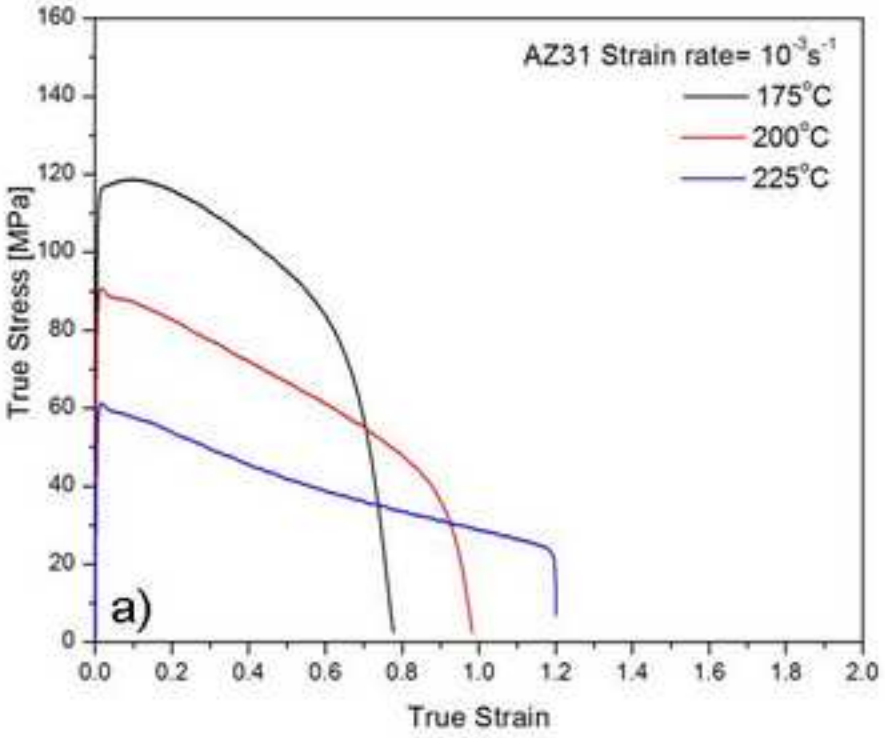

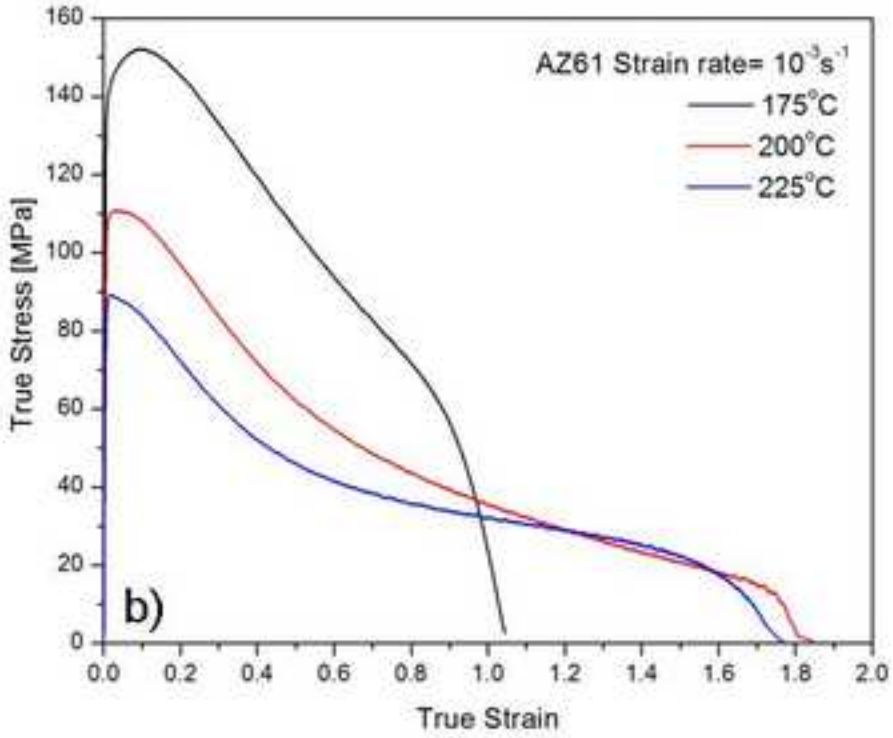

Figure(s)

Click here to download high resolution image

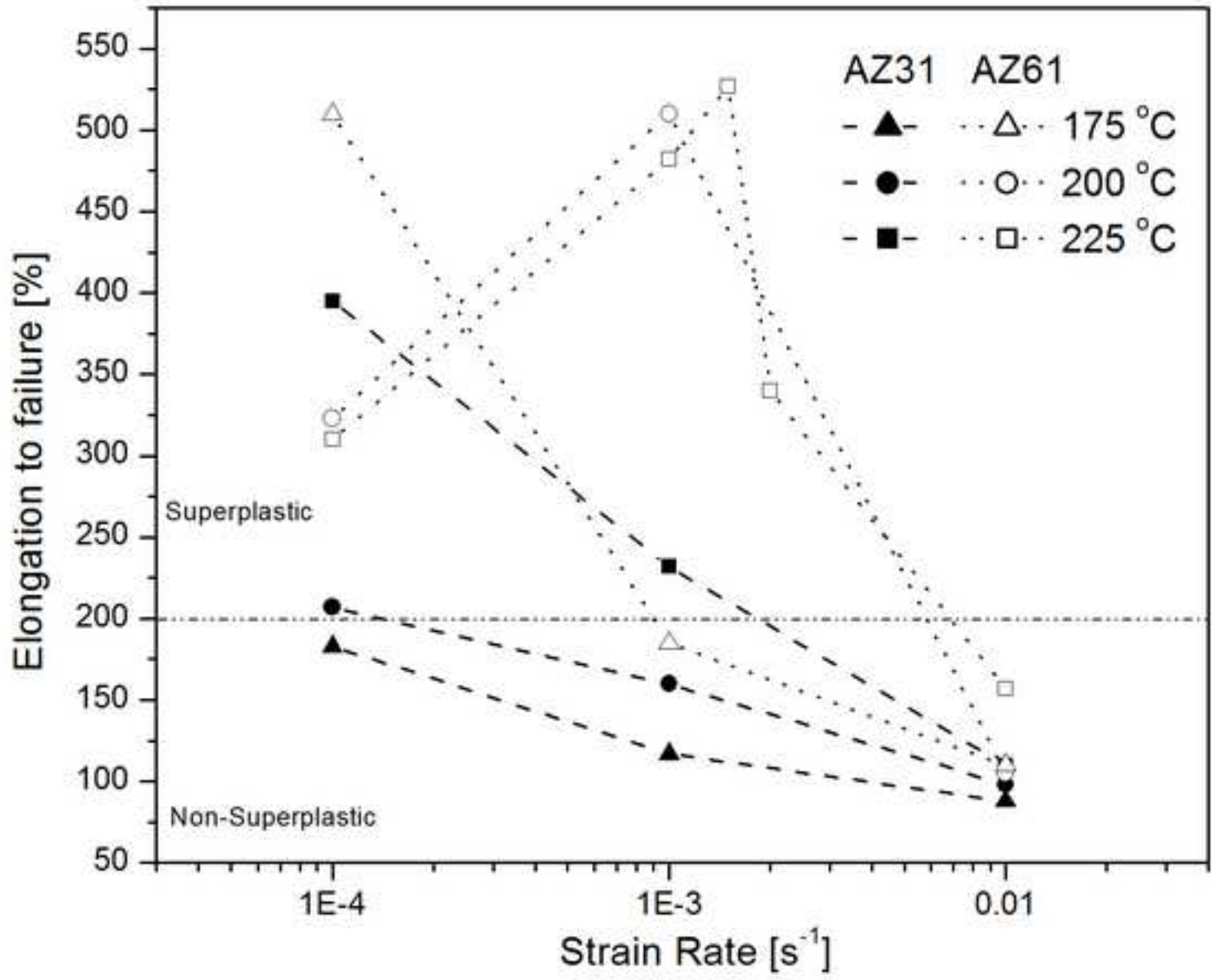

Figure(s)
Click here to download high resolution image

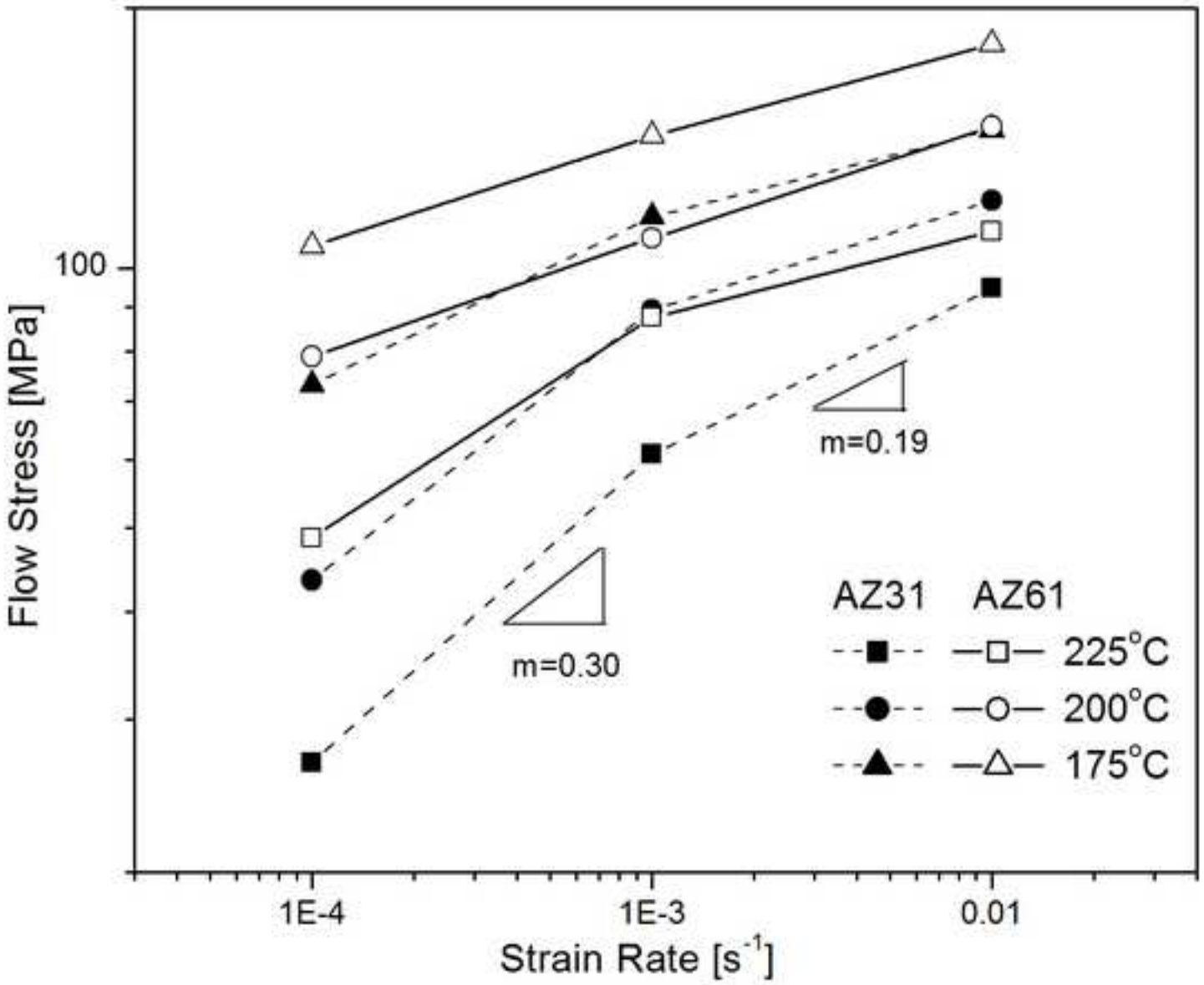

Figure(s)

Click here to download high resolution image

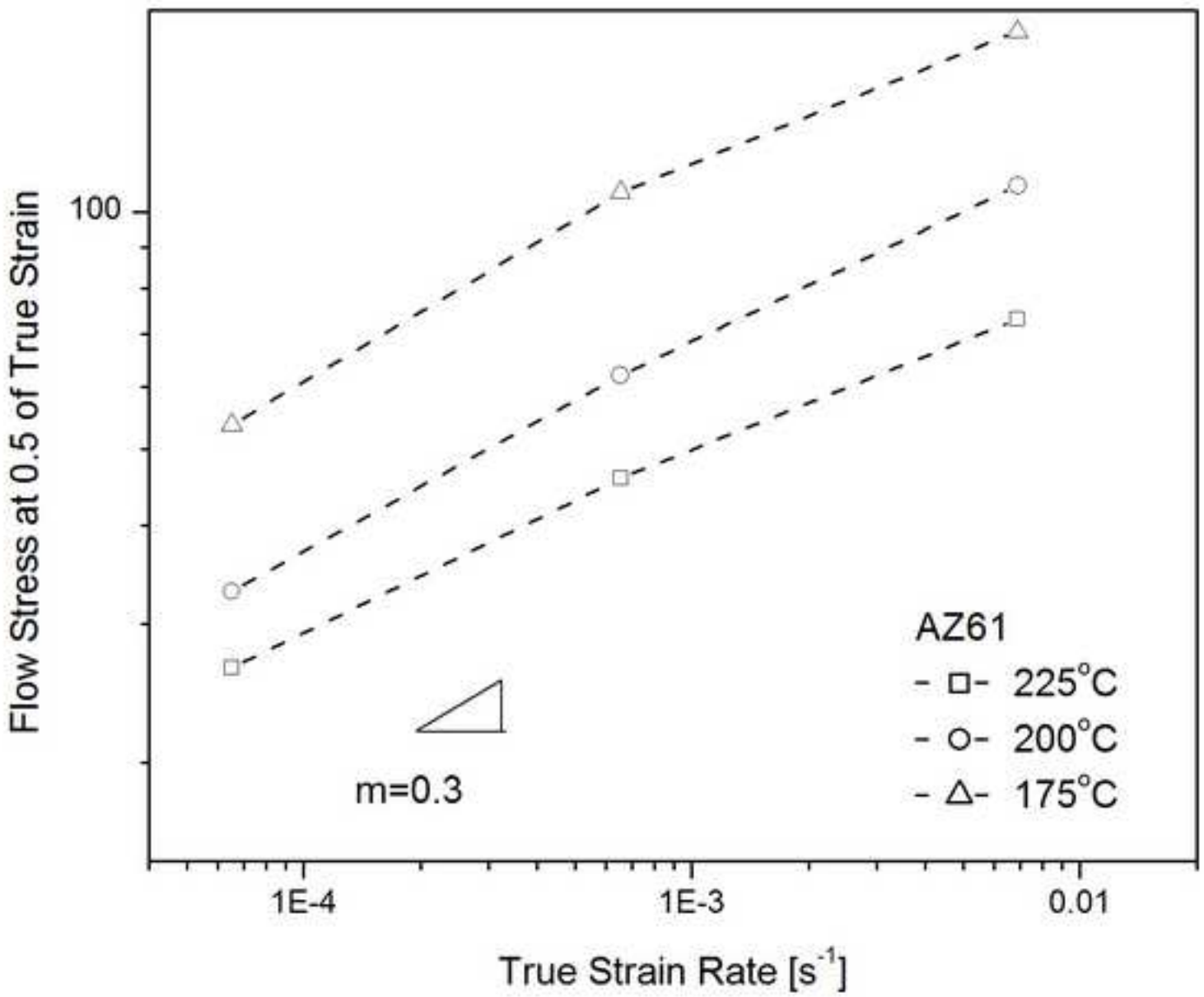

Figure(s)

Click here to download high resolution image

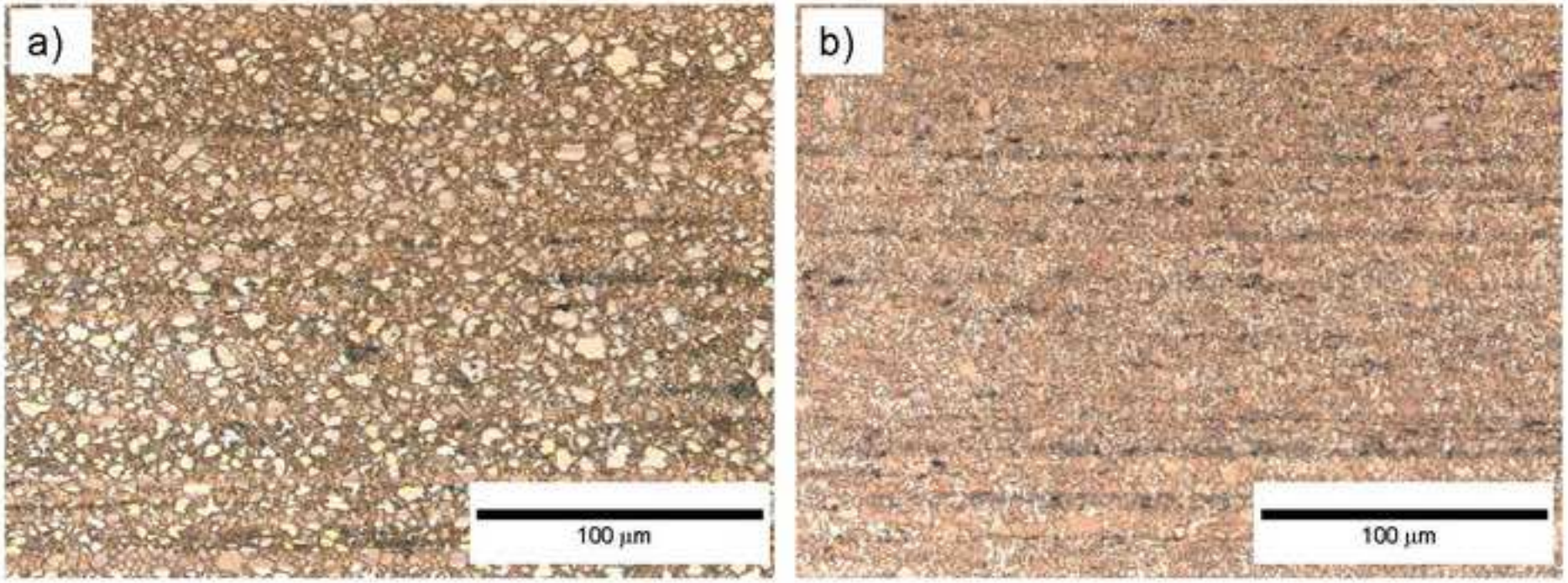

Figure(s)

Click here to download high resolution image

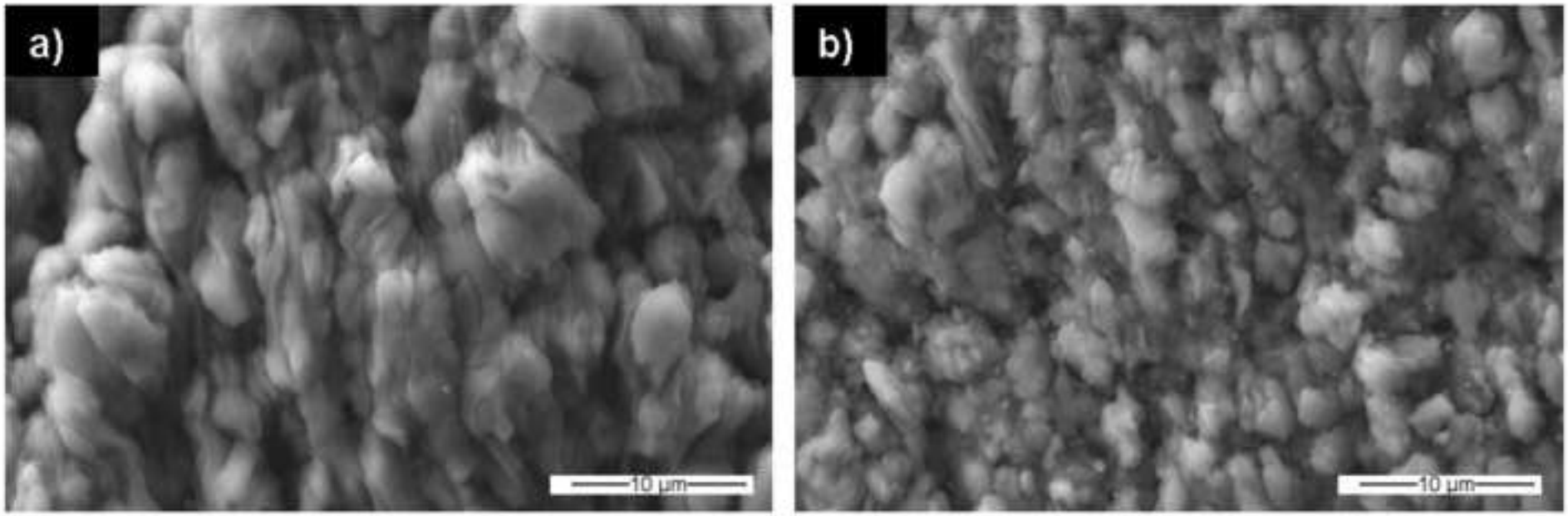

Figure(s)

Click here to download high resolution image

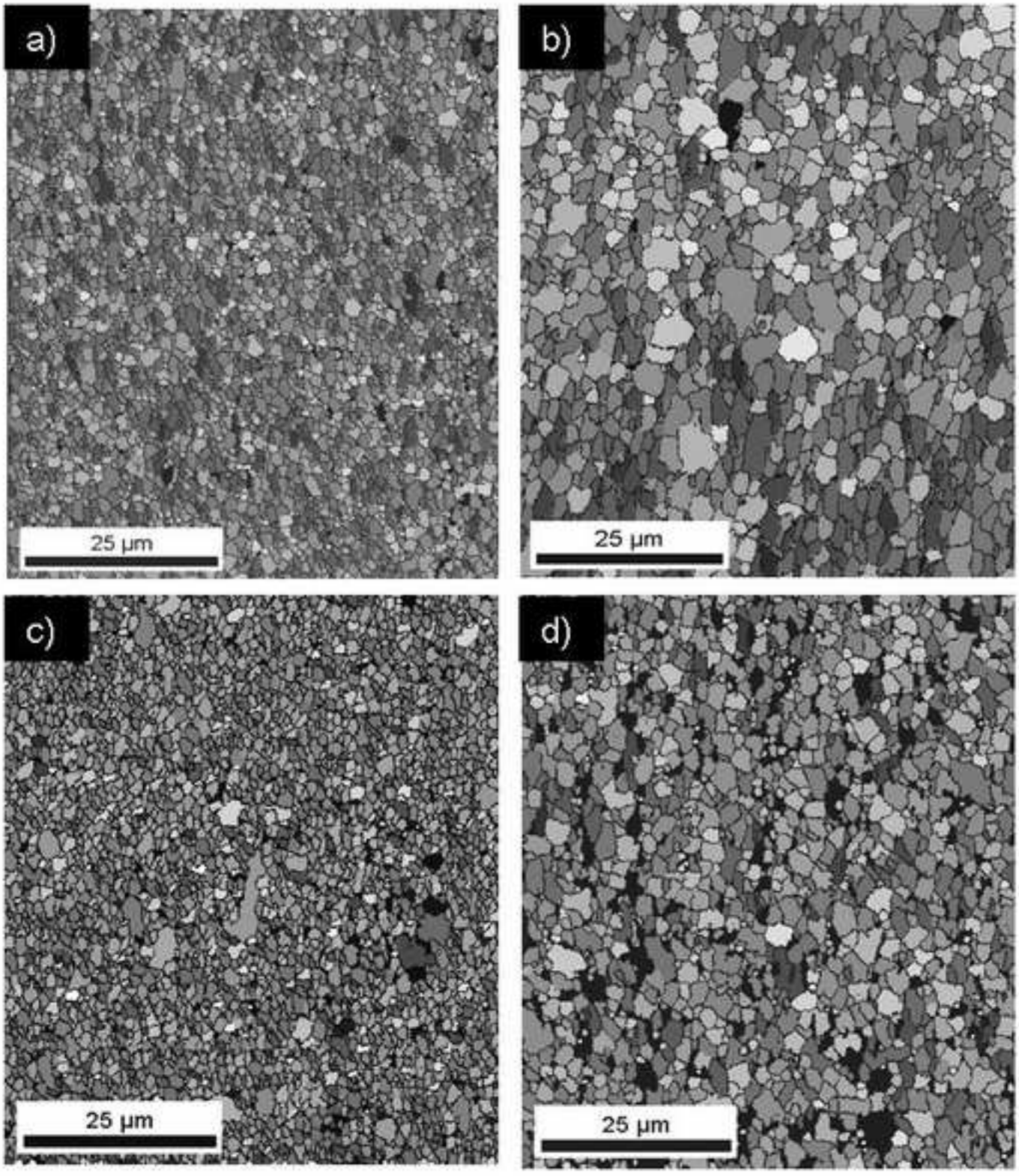

Figure(s)

Click here to download high resolution image

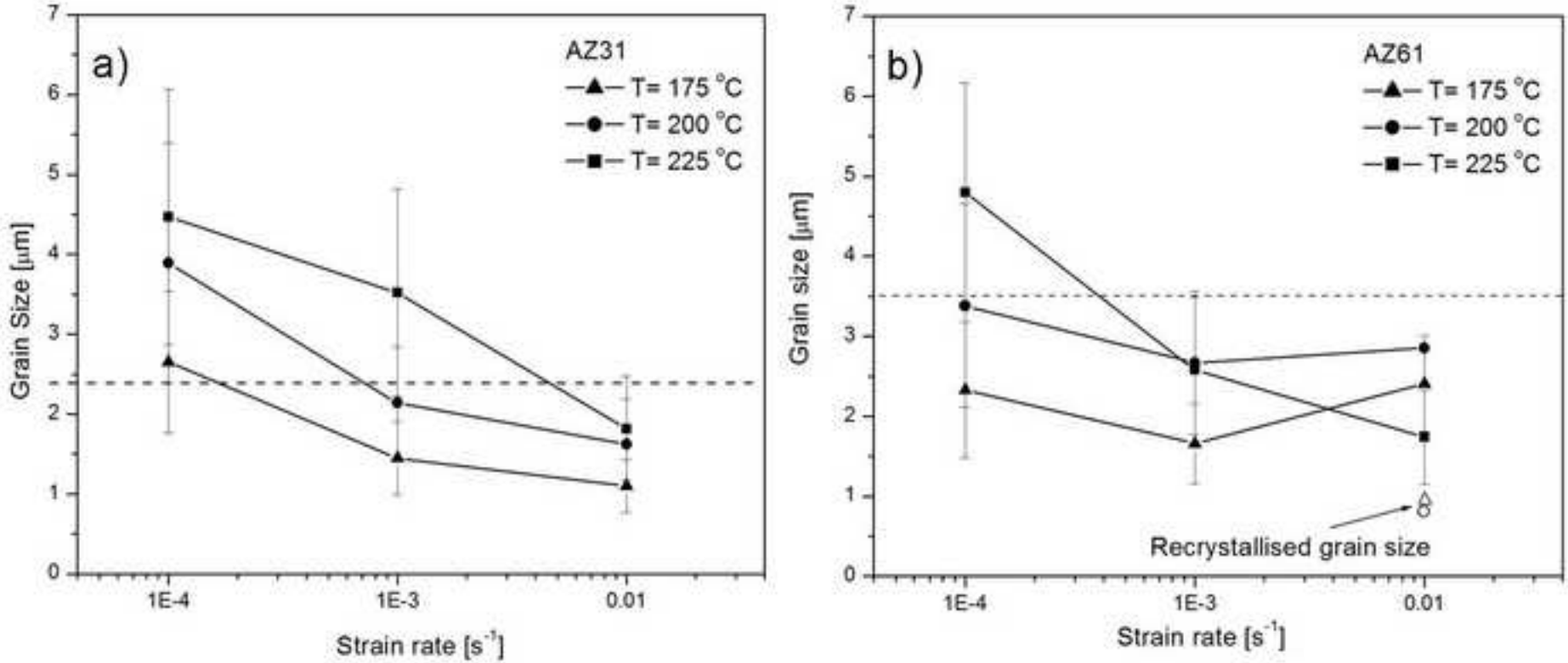

Figure(s)

Click here to download high resolution image

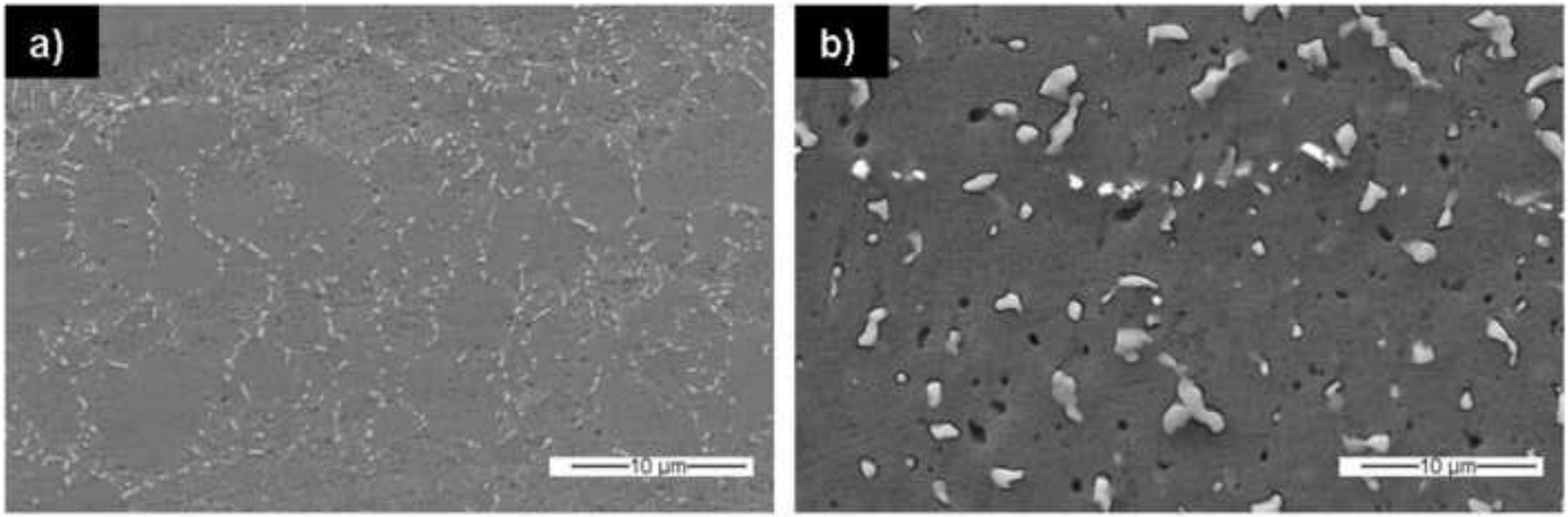

Figure(s)

Click here to download high resolution image